Soft Matter

Cite this: *Soft Matter*, 2012, **8**, 6931

www.rsc.org/softmatter

PAPER

Oscillatory shear-induced 3D crystalline order in colloidal hard-sphere fluids

T. H. Besseling,*[a] M. Hermes,†[a] A. Fortini,[b] M. Dijkstra,[a] A. Imhof[a] and A. van Blaaderen[a]

Received 11th November 2011, Accepted 24th April 2012
DOI: 10.1039/c2sm07156h

The non-equilibrium phase behavior of a colloidal hard-sphere fluid under oscillatory shear was investigated in real-space with experiments on poly(methyl methacrylate) (PMMA) colloidal suspensions and Brownian Dynamics computer simulations. All the samples in both experiments and the simulation are below the coexistence density of hard-sphere freezing, so the shear-induced crystals are out-of-equilibrium and melt after cessation of the shear. The physics is therefore fundamentally different from shear-induced crystallization in jammed or glassy systems. Although the computer simulations neglect hydrodynamic interactions and impose a linear flow, the results are in good agreement with the experiments. Depending on the amplitude and frequency of the oscillation, four regimes with different structures, hereafter referred to as phases, were identified: an oscillating twinned face-centered-cubic (fcc) phase, a sliding layer phase, a string phase and a phase that has not been reported previously in experiments, which we identify as tilted layers. This phase consists of lanes of particles that order in a hexagonal-like array (in the gradient-vorticity plane) which has lines of particles under an angle with the horizontal. Phases similar to the sliding layers, string phase and tilted layer phase were reported in Brownian and Molecular Dynamics simulations (systematically called string formation) but the validity of these simulations has been questioned. We demonstrate the experimental existence of these string-like phases and elucidate their structural differences in real-space.

Introduction

It is well known that shear has a large effect on colloidal self-assembly [1]. A remarkable example is that a hard-sphere fluid can crystallize as the result of oscillatory shear and that the shear-induced crystal melts back upon cessation of the shear [2,3]. These shear induced crystals are out-of-equilibrium and therefore the physics is fundamentally different from shear-induced crystallization in jammed or glassy systems [4,5]. Shear-induced crystallization is the result of flow-induced rearrangements in the micro-structure of the fluid, caused by an interplay between hydrodynamics interactions, Brownian motion and inter-particle forces. Understanding such complex flow behavior is industrially important and the possibility to switch between different states by means of an external field is promising for many applications (*e.g.* in the case of electronic ink when the switching is between a state displaying color by interference effects and one with less order and no color).

When subjected to steady shear, hard-sphere suspensions that are fluid in equilibrium do not display pronounced three-dimensional (3D) ordering for shear rates ranging from 10^{-3}–10^{2} s^{-1}. However, when oscillatory shear is applied to these samples, shear-induced ordering is observed such as layering,[6] string formation[7] and 3D crystal-like ordering.[3] The principal parameter governing the crystal-like ordering is the strain amplitude, which determines the distance of flow-induced interactions between the particles. For small strains, particles form hexagonal layers in the vorticity–velocity plane with one of the close-packed lines of particles perpendicular to the velocity direction. These layers slide from an ABC stacking at one extreme of the oscillation to an ACB stacking at the other, resulting in an oscillating twinned face-centered-cubic (fcc) crystal. For intermediate shear strain, the particles form hexagonal layers in the same plane as before, but now with one of the close-packed lines parallel to the velocity direction, and slide through the grooves of layers above and below. The oscillating twinned fcc phase and the sliding layer phase were observed with light scattering experiments on sheared hard-sphere suspensions[3] and on charged particles.[8,9] The same structural rearrangements were observed in real-space with suspensions that are above the bulk fluid coexistence density of hard spheres with optical and confocal microscopy[10–13] and with light scattering experiments.[3,14] Derks *et al.* showed for concentrated suspensions under steady shear that the close-packed lines of particles of the hexagonal layers align with the velocity direction and that the hexagonal layers slide over each other in a zig zag path, travelling from one triangular void of a neighboring layer to the other.[15]

[a]*Soft Condensed Matter, Debye Institute for NanoMaterials Science, Utrecht University, Princetonplein 5, 3584 CC Utrecht, The Netherlands. E-mail: t.h.besseling@uu.nl; a.vanblaaderen@uu.nl*
[b]*Theoretische Physik II, Physikalisches Institut Universität Bayreuth, D-95440 Bayreuth, Germany*
† Present address: School of Physics, The University of Edinburgh, Kings Buildings, Mayfield Road, Edinburgh EH9 3JZ, United Kingdom.

Non-equilibrium molecular dynamics (NEMD) simulations on oscillatory shear demonstrated the twinned fcc and sliding layer phases in samples that are fluid in equilibrium.[16,17]

For large strain amplitudes the hexagonal layers break up, resulting in strings of particles along the velocity direction, known as string formation. Weak string formation was observed in both steady and oscillatory shear experiments.[3,9] Early NEMD simulations on hard-sphere fluids under steady shear showed that at very high shear rates particles form strings in the direction of the flow and that these strings arrange in a regular hexagonal pattern in the gradient–vorticity plane.[18] More recent studies have argued that this string phase is an artifact arising from the assumed linear velocity profile and that a shear thickening regime without strings is observed instead,[19,20] consistent with experiments on PMMA colloids under steady shear.[21] However, non-equilibrium Brownian dynamics (NEBD) simulations on oscillatory shear revealed similar string-like ordering,[22] and the scattering diagram calculated from the string phase observed in the simulations strongly resembles the experimental light scattering results.[23] NEMD simulations that do not make any assumption about the velocity profile revealed oscillatory shear-induced ordering in a Lennard–Jones fluid but do not report on ordering in all three dimensions.[16] Of course, we are well aware of the fact that contrary to equilibrium behavior, the behavior of 'simple' and colloidal liquids under shear may be quite different.

We present a detailed, real-space study of oscillatory shear-induced order in hard-sphere colloidal fluids using both experiments on PMMA colloidal suspensions and NEBD simulations with an imposed linear velocity profile and no interparticle hydrodynamic interactions. The structure of an oscillating fcc and sliding layer phase, a string phase and a novel shear-induced phase not mentioned in the light scattering literature is presented together with its dependence on the strain amplitude and oscillation frequency.

Experimental methods and computer simulation

Particle characterization, shear cell setup, data acquisition

The particles used in this study were poly(methyl methacrylate) (PMMA) spheres with a diameter $\sigma = 2.07$ μm and a polydispersity of 3%, determined with static light scattering (SLS). They were sterically stabilized with poly(12-hydroxystearic acid) (PHS) gafted onto a PMMA backbone which was chemically attached to the core of the particles and covalently labeled with fluorescent rhodamine isothiocyanate (RITC) dye for imaging.[24] Particles were dispersed in a 26 wt% mixture of *cis*-decahydronaphtalene (*cis*-decalin) in cyclohexyl bromide (CHB) saturated with the salt tetrabutylammonium bromide (TBAB). This mixture nearly matches the density of the particles ($\rho = 1.19$ g ml^{-1}) and also closely matches the index of refraction ($n_D^{25} = 1.492$). The viscosity of the solvent mixture was 2.2 mPa s.[25] The high salt concentration screens the charges on the particles, making them behave approximately as hard spheres.[26]

The equilibrium phase behavior of the suspension was determined by filling five capillaries with different weight fractions of the sterically stabilized PMMA particles (0.388, 0.408, 0.419, 0.427 and 0.438). Because the particles were nearly density matched, these weighted values are approximately equal to the dry PMMA volume fraction ϕ_c. The capillaries were stored horizontally in a temperature controlled room at 21 ± 1 °C and after 22 h the particle positions were determined over the complete height of the capillary with confocal microscopy. The fraction of particles that are part of a crystal was determined by bond order parameter analysis (described later in this section) and plotted in Fig. 1. Since the particles were closely density matched, sedimentation did not have a significant effect during the 22 h. With linear regression, an average scaling factor $p = 1.23 \pm 0.01$ was determined that maps the values in Fig. 1 onto the hard-sphere phase diagram,[27] resulting in a freezing point $\phi_c = 0.40 \pm 0.01$ and melting point $\phi_c = 0.44 \pm 0.01$. The effective particle diameter was on average $1.23^{1/3} = 1.07$ times larger than determined with SLS. This is because the particles absorb some of the CHB, causing them to swell, combined with leftover charge effects.[26] The effective diameter was also measured by determining the distance of nearest approach from the first peak in the pair correlation function $g(r)$ of a crystalline domain in the coexistence region. Using the hard-sphere melting point ($\phi = 0.54$) as reference, this resulted in an effective particle diameter of 1.05σ, which is slightly smaller than that obtained with the previous method.

A parallel plate shear cell mounted on top of an inverted confocal microscope was used to investigate the real-space behavior of particles under shear.[28] Fig. 2 shows a schematic of the shear cell and our choice of the coordinate system. The top and bottom plate are microscopy glass slides attached to translational cassettes that can be displaced with piezostepper motors. Alignment of the glass slides was performed using confocal microscopy in reflection mode using an HeNe 543 nm laser and an air objective (20x 0.7 NA, Leica). The slides varied by ~1 μm in the z-direction over the full travel of 1 cm (0.01%) based on extensive testing of the setup.[28] The typical spacing between the slides was 100 μm and an amount of ~60 μL of suspension was placed between the slides to fill the cell. A metal vapor lock was used to prevent evaporation of the suspending liquid. The amplitude A, velocity v_{max} and gap width h (typically 100 μm) determine the maximum strain amplitude $\gamma_{max} = 2A/h$ and the maximum shear rate $\dot{\gamma}_{max} = 2v_{max}/h$.[29] The time dependent shear rate and strain amplitude are given by

$$\gamma(t) = \gamma_{max}\sin(2\pi f t) \quad (1)$$

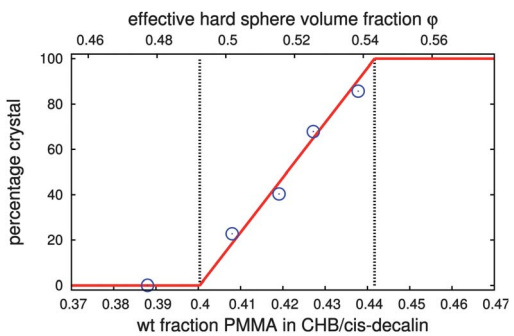

Fig. 1 The equilibrium phase behavior as a function of dry weight fraction PMMA in CHB/*cis*-decalin, 22 h after dispersing the particles. An average scaling factor $p = 1.23 \pm 0.01$ maps the system onto the hard-sphere phase diagram.

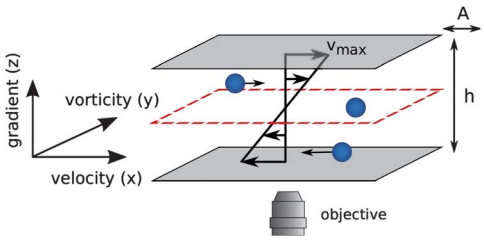

Fig. 2 Shear cell schematic and coordinate system definition. The amplitude A, maximum velocity v_{max} and height h is set during the experiment. The red dotted line indicates the plane of zero velocity.

$$\dot{\gamma}(t) = \dot{\gamma}_{max}\cos(2\pi f t), \tag{2}$$

with f the frequency of oscillation and $\dot{\gamma}_{max} = 2\pi f \gamma_{max}$. We define the Peclet number Pe as

$$Pe = \frac{\dot{\gamma}_{max}\,\eta\, a^3}{k_B T}, \tag{3}$$

with $a = \sigma/2$ the particle radius and η the viscosity of the medium.

Digital images of the colloidal dispersion were obtained with a confocal scanning laser microscope (Leica TCS SP2) and an oil immersion objective (100x 1.4 NA, Leica). The RITC labeled particles were excited with an HeNe 543 nm laser and a piezo focusing drive (Physik Instrumente) was used for scanning in the vertical direction. Measurements were performed in a temperature controlled room at 21 ± 1 °C. The coordinates of the particles were obtained using an algorithm similar to the method described by Crocker and Grier,[30] but extended to 3D as *e.g.* schematically described in ref. [31].

Simulation method

Non-equilibrium Brownian Dynamics (NEBD) simulations were used to model colloidal particles of diameter σ under shear. The unit of time is the Brownian relaxation time $\tau_B = a^2/D_0$, with $a = \sigma/2$ the radius of the colloidal particles and $D_0 = k_B T/\xi$ the bare diffusion constant, k_B the Boltzmann constant, T the temperature and ξ the Stokes drag coefficient. We define $\xi = 6\pi\eta a$ as the unit of drag which fixes the viscosity η. For particles with diameter $\sigma = 2.07$ μm, the unit of time $\tau_B = 11.3$ s, the drag coefficient $\xi = 4.3 \times 10^{-8}$ N s m^{-1} and the unit of energy $k_B T = 4.1 \times 10^{-21}$ J. The simulations were carried out in a simulation box with periodic boundary conditions in the x and y directions and two walls positioned at $z = 0$ and $z = h$. The number of particles varied between 1200 and 3456 and the shape of the box was chosen to be commensurate with the dimensions of the expected crystalline phases. To approximate hard-sphere-like particles, an inverse power law was used for the pair-wise interaction potential

$$U_{ij}(r) = \varepsilon\left(\frac{\sigma}{r}\right)^{36}, \tag{4}$$

with ε the interaction energy, σ the particle diameter and $r \equiv |\mathbf{r}_i - \mathbf{r}_j|$ the center-of-mass distance between particles i and j. For efficiency reasons this potential was truncated at 1.02σ and shifted to make it continuous. The wall–particle interaction is taken to be

$$U_{wall} = \begin{cases} \varepsilon_w\left(\dfrac{\sigma}{z}\right)^6 & \text{for } z < \sigma/2 \\ \varepsilon_w\left(\dfrac{\sigma}{h-z}\right)^6 & \text{for } z > h - \sigma/2 \\ 0 & \text{otherwise} \end{cases} \tag{5}$$

with ε_w the wall–particle interaction energy and z the z-coordinate of a particle. We used the integration method of Ermak[32] with an additional term to account for the oscillating shear

$$\mathbf{r}_i(t+\delta t) = \mathbf{r}_i(t) + \delta t\frac{-\nabla U_i(t)}{\xi} + \delta\mathbf{r}_i^G + \delta t\dot{\gamma}(t)z_i(t)\hat{\mathbf{x}}, \tag{6}$$

with $-\nabla U_i$ the force acting on the particle as a result of the potential energy, $\delta\mathbf{r}_i^G$ a Gaussian random displacement with zero mean and variance $\langle(\delta r_{i\alpha}^G)^2\rangle = 2D_0\delta t$ where $\alpha \in \{x, y, z\}$. The term $\dot{\gamma}(t)z_i(t)\hat{\mathbf{x}}$ imposes a linear velocity profile on the system. Previous experimental work by Wu *et al.*[33] has shown that the velocity profile of a partially crystallized (or sliding layer) suspension deviated from linearity and that the local shear rate is approximately 1.5 times higher in the layered region than in the fluid phase. In the simulations we neglect these deviations from a linear profile because we expect that they do not strongly effect the shear induced structures. The time step δt used to evaluate eqn (6) was chosen to be much larger than the velocity relaxation time ($\sim m/\xi$), but much smaller than the Brownian relaxation time (a^2/D_0). It is important to note that hydrodynamic interactions, which are neglected in Brownian dynamics simulations, become more important for larger shear rates and higher volume fractions[34] and that they also play an important role in determining the absolute time scales in the system.

Structure analysis

The local hexagonal order in a single plane is quantified with the absolute value of the 2D local bond order parameter ψ_6 given by

$$|\psi_6(i)| = \left|\frac{1}{n_c(i)}\sum_{j=1} n_c(i)e^{i6\theta(\mathbf{r}_{ij})}\right|, \tag{7}$$

with $n_c(i)$ the number of nearest neighbors of particle i, which is defined as the number of particles that are within a distance of 1.4σ of the particle, $\mathbf{r}_{ij}$ the vector connecting particles i and j, $\theta(\mathbf{r}_{ij})$ the angle between $\mathbf{r}_{ij}$ and some arbitrarily chosen reference axis, and the i in the exponent the imaginary unit. In a perfect hexagonal layer, the angles $\theta(\mathbf{r}_{ij})$ are multiples of 60° and $|\psi_6(i)| = 1$. To quantify the 2D global hexagonal order we used the global order parameter Ψ_6, given by

$$\Psi_6 = \left|\frac{\sum_{i=1}^{N}\psi_6(i)}{N}\right|, \tag{8}$$

with N the number of particles in the plane. For a dense hard-sphere fluid, this order parameter vanishes in the limit of an infinitely large system size ($\lim_{N\to\infty}\Psi_6 = 0$).

To quantify the symmetry of three dimensional local structure surrounding a particle, the method of local bond orientational order parameters was followed.[35] Based on the spherical harmonics Y_{lm}, a set of numbers was computed for each particle

$$q_{lm}(i) = \frac{1}{n_c(i)} \sum_{j=1}^{n_c(i)} Y_{lm}(\hat{\mathbf{r}}_{ij}), \tag{9}$$

with l an integer parameter and m an integer running from $-l$ to l. The unit vector $\hat{\mathbf{r}}_{ij}$ connects particle i and one of its nearest neighbors j. To distinguish between particles that are in a liquid-like environment and particles that are in a crystal-like environment we used the method described by Ten Wolde *et al.*[36] A normalized complex vector $\mathbf{q}_l(i)$ was constructed with $(2l + 1)$ components $\tilde{q}_{lm}(i)$ that are proportional to the numbers $q_{lm}(i)$. Next, the correlation between the vector $\mathbf{q}_l(i)$ and the vector of its nearest neighbor $\mathbf{q}_l(j)$ was computed by defining the scalar product

$$\mathbf{q}_l(i) \cdot \mathbf{q}_l(j) = \sum_{m=-l}^{l} \tilde{q}_{lm}(i)\, \tilde{q}_{lm}(j)^*. \tag{10}$$

If the local structures of particle i and j are similar, the value of the scalar product is close to one and a crystal-like bond was assigned to the particles. Because thermal broadening results in a distribution of values, it is necessary to define a threshold value for the scalar product. As we expect the crystal to have hexagonal order, we chose a symmetry index $l = 6$. We used a threshold value of 0.7 and because some particles in the fluid phase exceed this threshold, a particle was called crystal-like only if in addition it had a minimum of 8 crystalline bonds.

The structure factor $S(\mathbf{q})$ was calculated according to

$$S(\mathbf{q}) = \frac{1}{N} \left\langle \sum_{j=1}^{N} \sum_{k=1}^{N} e^{i\mathbf{q}(\mathbf{r}_k - \mathbf{r}_j)} \right\rangle, \tag{11}$$

with N the number of particles in the sample and the angular brackets denoting an ensemble average. The vector $\mathbf{q}$ was chosen such that $q_\alpha = 2\pi n/L_\alpha$ with n an integer, $\alpha \in \{x,y,z\}$ and L_α the system size. A cosine window was used to avoid artefacts caused by the shape of the box.

Results

We studied oscillatory shear-induced ordering in fluid samples with volume fractions in the range $\phi = 0.46$–0.49, *i.e.* just below the freezing point. First, we describe the different ordered phases that were observed when the frequency and amplitude of the oscillatory shear were varied, both in the experiments and in the simulations. We discuss to what extent these phases agree with previous work, which was mainly done with light scattering techniques. Finally, we map out a non-equilibrium phase diagram.

Twinned fcc

The structural changes that can be observed in the fluids under shear are rich and strongly dependent on the strain amplitude. In Fig. 3A a suspension with a volume fraction $\phi = 0.47 \pm 0.01$ is shown. Without shear, the sample remained in the fluid phase and for strain amplitudes $\gamma_{max} \leq 0.1$ no shear-induced order was observed for any frequency. Fig. 3B shows that for a strain amplitude $\gamma_{max} = 0.36$ and frequency $f = 4.5\ \tau_B^{-1}$ ($Pe = 0.5$) the particles formed hexagonal layers in the velocity–vorticity plane with a close packed direction (indicated by the lines of particles

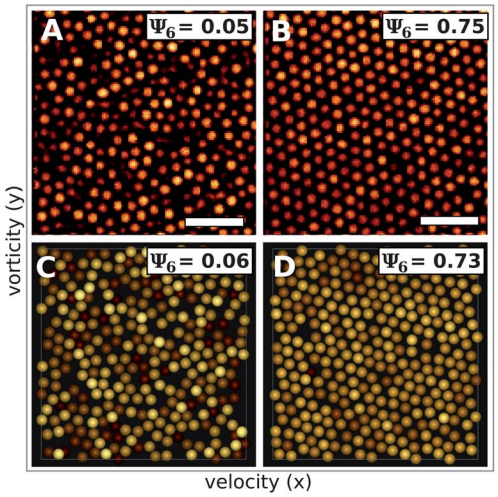

Fig. 3 Shear-induced crystallization with perpendicular alignment, observed in the velocity–vorticity plane. Values of the global hexagonal order parameter Ψ_6 are indicated in the figures. (A, B) Experimental results for a sample with volume fraction $\phi = 0.47 \pm 0.01$. Scale bars are 10 μm. (A) The quiescent sample is fluid in equilibrium. (B) When subjected to shear with strain amplitude $\gamma_{max} = 0.36$ and frequency $f = 4.5\ \tau_B^{-1}$, particles form hexagonal layers with one of the close packed directions almost perpendicular to the velocity direction. (C, D) Simulation results for $\phi = 0.49$. The figures show a part of the simulation box with particles color coded according to their z-position. (D) For $\gamma_{max} = 0.35$ and $f = 4.3\ \tau_B^{-1}$, the ordering is almost identical to that of the experiment.

forming the 2D hexagonal arrangement) almost perpendicular to the velocity. Fig. 3C shows a snapshot of a simulation with a volume fraction $\phi = 0.49$ and the particles color coded according to their z-position, so they appear brighter the closer they are to the plane. After the application of a shear with $\gamma_{max} = 0.35$ and $f = 4.3\ \tau_B^{-1}$ (again $Pe = 0.5$), almost identical ordering compared to the experiments was observed (Fig. 3D). The insets show the increase in the values of the global hexagonal order parameter Ψ_6. Note that both in the experiments and simulations a slight deviation of the close packed lines with respect to the vorticity direction was found. Similar small but systematic deviations were also found for the crystalline structures described below.

To determine the stacking of these hexagonal layers, confocal images of the gradient–velocity plane were taken directly after cessation of the shear and compared with the simulations. Fig. 4 shows images taken at different moments of the oscillation cycle for $\gamma_{max} = 0.3$ and $f = 10.0\ \tau_B^{-1}$ (experiment) and $f = 50.0\ \tau_B^{-1}$ (simulation) after application of shear for 1200 oscillations. The higher frequency in the simulation was used for efficiency reasons. The crystal-like particles in the simulation snapshots are colored red and the fluid-like particles are colored cyan. Both types of particles are reduced in diameter (0.5σ and 0.2σ, respectively) to enhance visualization. In Fig. 4A the oscillation is at maximum displacement and the layers are ABC stacked, indicating an fcc phase. At the equilibrium position of the oscillation (Fig. 4B), the layers are bridge-site stacked and a body-centered-tetragonal (bct) phase is temporarily formed. At the other maximum displacement (Fig. 4C), the particles are

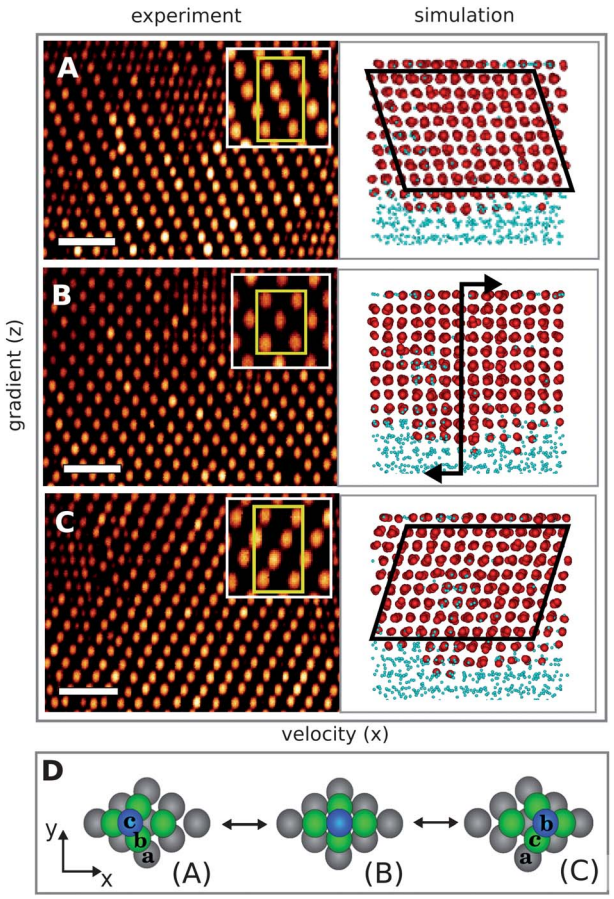

Fig. 4 Oscillating fcc phase in the velocity–gradient plane. Experimental results (left) for $\phi = 0.46 \pm 0.01$, $\gamma_{max} = 0.3$ and $f = 10.0\ \tau_B^{-1}$ after 1200 oscillations. The scale bars indicate 12 μm. Simulation results (right) for $\phi = 0.49$, $\gamma_{max} = 0.3$ and $f = 50.0\ \tau_B^{-1}$, again after 1200 oscillations. Crystal particles are colored red and reduced to 0.5σ, fluid particles are colored cyan and reduced to 0.2σ to enhance visualization. (A) Particles are fcc stacked (ABC) at the maximum displacement of the plates. (B) The hexagonal layers are bridge-site stacked, corresponding to a bct phase. (C) Particles are twin stacked at the other maximum displacement of the plates (ACB). (D) Schematic model of the relative movement of the layers during shear.

again fcc stacked, but with the other twin structure (ACB). The schematic drawing in Fig. 4D shows that this transition in stacking can be explained with a simple geometrical model where the particles oscillate between two neighboring triangular voids, as proposed originally by Ackerson.[3] It is likely that this movement enables the particles to minimize the stress caused by collisions with other particles during the shear. From both the experiments and the simulations it is clear that for small strain amplitudes a twinned fcc-like phase is formed in an initial hard-sphere fluid. In both experiments and simulations we always observed the crystal together with a fluid phase. The strain amplitude that corresponds to the exact dimensions of an fcc crystal is given by $\gamma_{max} = \Delta x/\Delta z = 0.35$, with Δx the distance between two neighboring voids and Δz the distance between two hexagonal layers. For lower volume fractions, the fcc phase can persist for significantly larger strain amplitudes because of the larger free volume. A simple geometrical calculation shows that for $\phi = 0.49$, the strain amplitude has to be larger than $\gamma_{max} = 0.69$ before particles in a perfect fcc crystal touch during the oscillatory motion.

To further demonstrate the twinning behavior, particle coordinates were obtained from experiments with $\gamma_{max} = 0.3$, $f = 10.0\ \tau_B^{-1}$ and $\phi = 0.47 \pm 0.01$. In Fig. 5A the rendered particles are shown at the two extremes of the oscillation directly after cessation of the shear. Again, crystal-like particles are shown in red, fluid like particles are shown in cyan and both are reduced in diameter to enhance visualization. Fig. 5B shows plots of the calculated 3D structure factor $S(\mathbf{q})$ in the q_x–q_y plane, confirming the twinning behavior. The light scattering experiments by Ackerson on hard-sphere fluids under oscillatory shear reveal the same position of the diffraction peaks as in Fig. 5B, although the maxima are spread out around the inner ring instead of appearing as small spots.[3] This was also observed for soft spheres[8] and for samples above the bulk fluid coexistence density,[10,14] indicating a distribution of crystalline domains centered at the vorticity direction.

Sliding layers

When the strain amplitude exceeds approximately 0.5, collisions between particles will prevent the formation of the twinned fcc phase, and particles form hexagonal layers aligned parallel to the velocity direction. In Fig. 6, experimental results are shown for a quiescent sample (Fig. 6A) and after application of shear with strain amplitude $\gamma_{max} = 0.6$ and frequency $f = 2.5\ \tau_B^{-1}$ ($Pe = 0.5$, Fig. 6B) after approximately 100 oscillations. Simulation snapshots are shown before (Fig. 6C) and after shear with $\gamma_{max} = 0.8$ and $f = 3.7\ \tau_B^{-1}$ ($Pe = 1.0$, Fig. 6D) after 200 oscillations. The high values of the global order parameter Ψ_6 in Fig. 6B and Fig. 6D are a clear indication of the hexagonal ordering in the velocity–vorticity plane.

A comparison between the stacking of hexagonal layers observed in the experiments and with simulations is shown in Fig. 7. The experimental results are from a suspension with volume fraction $\phi = 0.47 \pm 0.01$, $\gamma_{max} = 1.3$ and $f = 4.1\ \tau_B^{-1}$. The

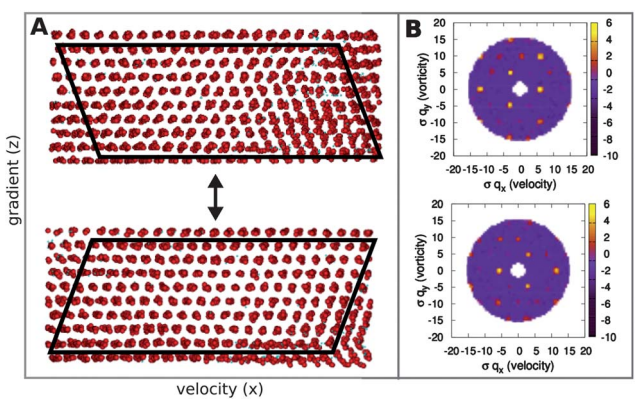

Fig. 5 Experimental results on the twinned fcc phase. (A) Rendered particle positions at both extremes of the oscillation, after applying shear with $\gamma_{max} = 0.3$ and $f = 10.0\ \tau_B^{-1}$ to a suspension with volume fraction $\phi = 0.47 \pm 0.01$. Red indicates crystal-like particles and cyan indicates fluid order. The particles are reduced in diameter to enhance visualization. (B) The calculated 3D structure factor $S(\mathbf{q})$ at both extremes of the oscillation in the q_x–q_y plane demonstrates the twinning behavior.

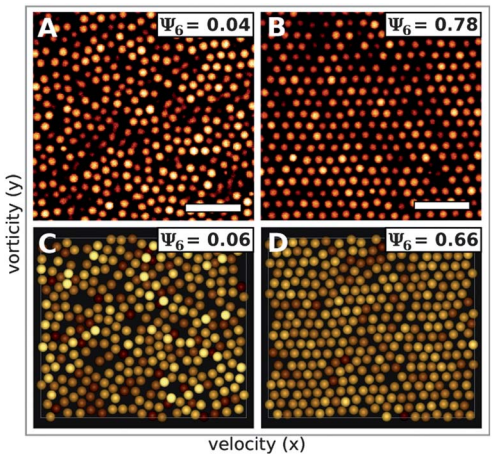

Fig. 6 Formation of the sliding layer phase. (A, B) Experimental results for ordering in a sample with volume fraction $\phi = 0.47 \pm 0.01$ before and after application of shear with strain amplitude $\gamma_{max} = 0.6$ and frequency $f = 2.5\ \tau_B^{-1}$. Scale bars are 10 μm. (C, D) Simulation snapshots for $\phi = 0.49$, $\gamma_{max} = 0.8$ and frequency $f = 3.7\ \tau_B^{-1}$. Particles are color coded according to their z-position. Values of the global hexagonal order parameter Ψ_6 are indicated in the figure.

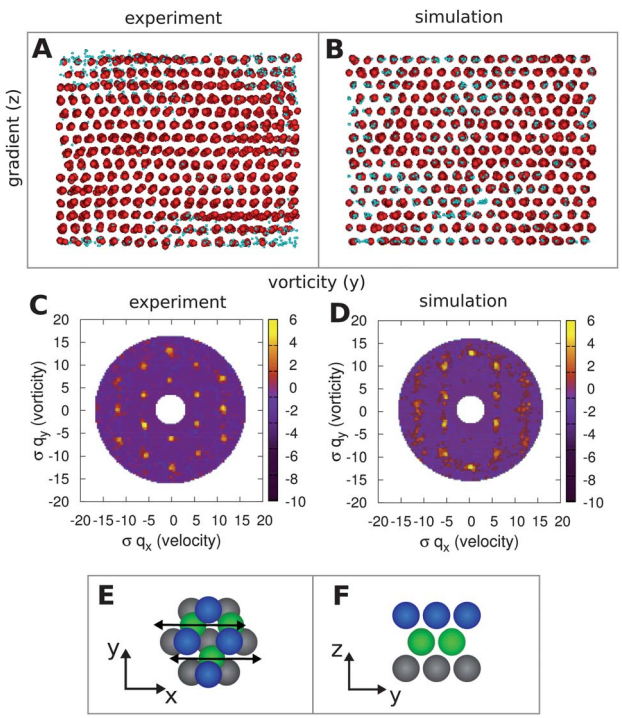

Fig. 7 Structure of the sliding layer phase. Experimental results for $\gamma_{max} = 1.3, f = 4.1\tau_B^{-1}$ and $\phi = 0.47 \pm 0.01$ and simulation for $\gamma_{max} = 1.2$, $f = 10.0\ \tau_B^{-1}$ and $\phi = 0.49$. Crystal particles are shown in red and fluid particles in cyan. Both are reduced in diameter to enhance visualization. (A) After cessation of the shear, random stacked layers were found in the experiments. (B) Viewed from the vorticity–gradient plane, every third hexagonal layer is positioned on top of the first in the simulations. The structure factor $S(\mathbf{q})$, calculated from 3D coordinates, indicates (C) random stacked layers and (D) sliding layers. (E, F) Proposed movement of the layers during shear.

particle coordinates in Fig. 7A were obtained from a 3D stack of images taken directly after the cessation of the shear and the structure factor $S(\mathbf{q})$ shown in Fig. 7C is calculated from these 3D coordinates. The view from the vorticity–gradient plane in Fig. 7A shows random stacking of the layers, which is confirmed by the hexagonal pattern in Fig. 7C. The simulation snapshot in Fig. 7B is for $\phi = 0.49$, $\gamma_{max} = 1.2$ and $f = 10.0\ \tau_B^{-1}$ and shows that every third layer is positioned on top of the first, when viewed from the vorticity–gradient plane. The fourfold pattern of the corresponding structure factor (Fig. 7D) resembles the pattern observed by Ackerson with light scattering experiments,[3,9] who argued that if the volume fraction $\phi < 0.58$, the hexagonal layers can slide in straight lines through the grooves formed by a neighboring layer, as indicated in Fig. 7E. The consequence of this movement is that the registry (in terms of the close packed stacking points ABC) between the layers vanishes and the resulting phase is called the freely sliding layer phase.[3] Fig. 7F shows that the view of the sliding layer phase in the vorticity–gradient plane is indeed very similar to what is found in the simulations (Fig. 7B).

The six-fold pattern in Fig. 7C is expected for higher volume fractions $\phi > 0.58$ when there is still registry between the layers. From these observations we conclude that in the experiments, particles rearranged after cessation of the shear into the triangular voids of neighboring layers during the time it takes to acquire the confocal images, which resulted in randomly stacked layers.

String phase

For increasing strain amplitude, decreasing Peclet number and decreasing volume fraction we observed a systematic decrease of

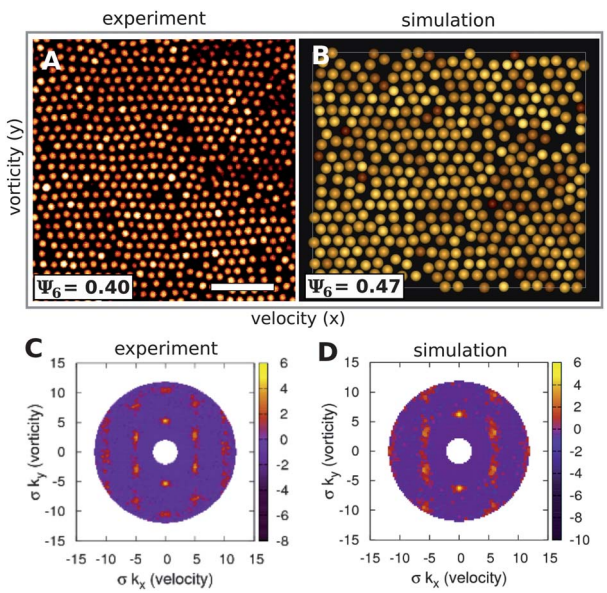

Fig. 8 The string phase. (A) Confocal image with $\phi = 0.46 \pm 0.01$, $\gamma_{max} = 1.2$ and $f = 2.5\ \tau_B^{-1}$ ($Pe = 1.0$). The scale bar is 15 μm. (B) Simulation snapshot after application of shear with the same strain amplitude and frequency as in (A) and with volume fraction $\phi = 0.48$. The values for the global order parameter Ψ_6 are indicated in the figures. The structure factors $S(\mathbf{q})$ in (C) and (D) are calculated from 2D coordinates obtained from (A) and (B) respectively and indicate the string-like order in both systems.

the global order parameter Ψ_6, indicating a deviation from hexagonal symmetry. This deviation is demonstrated in Fig. 8A (experiment) and in Fig. 8B (simulation), both after application of shear with $\gamma_{max} = 1.2$ and $f = 2.5\ \tau_B^{-1}$ ($Pe = 1.0$). The ordering in Fig. 8A looks hexagonal, but by careful inspection it shows strings of particles along the velocity direction with regular spacing within the strings but with little long-range correlation between the strings, which is confirmed by the fact that the lines of close packed particles other than those parallel to the velocity are not straight. This type of ordering is reflected in the values of the order parameters. Because many particles have six neighbors more or less hexagonally distributed around them, the average local order parameter in Fig. 8A is high ($\langle|\psi_6(i)|\rangle = 0.70$). However, because the layer lacks long-range order, the global order parameter is low ($\Psi_6 = 0.40$) compared to the value for the sliding layer phase shown in Fig. 6B ($\Psi_6 = 0.78$). A similar but less pronounced trend was found for the simulation snapshot shown in Fig. 8B ($\langle|\psi_6(i)|\rangle = 0.66$ and $\Psi_6 = 0.47$). Because the string-like phase in Fig. 8A started to melt back the moment the shear was stopped, it was impossible to acquire 3D particle coordinates, again in stark contrast with the sliding layer phase. Therefore, the structure factors in Fig. 8C (experiment) and Fig. 8D (simulation) were calculated from 2D coordinates. The broadening of the intensity maxima along the vorticity direction is a direct consequence of the string-like ordering of the particles and corresponds well to the string phase scattered intensity distribution of Ackerson.[3]

We found no sharp transition between the sliding layer phase and the string phase and planes with high values of the global order parameter ($\Psi_6 \gtrsim 0.60$) and low values were often observed in the same simulation box. The ordering in the gradient–vorticity plane strongly resembled the pattern for the sliding layer phase (Fig. 7B).

Tilted layer phase

For both large strain amplitudes and high frequencies (*i.e.* high Peclet numbers), a fourth shear-induced 3D structure or phase was observed that is remarkably different from the others in that it does not consist of layers of particles parallel to the velocity–vorticity plane. Fig. 9 shows the experimental measurements corresponding to $\gamma_{max} = 0.65$ and $f = 70.0\ \tau_B^{-1}$ ($Pe = 15$) after 500 oscillations and simulations with $\gamma_{max} = 0.9$ and $f = 50.0\ \tau_B^{-1}$ (also $Pe = 15$) after 200 oscillations. In Fig. 9A, particles are shown in the velocity–vorticity plane during the shear, whilst Fig. 9B shows a simulation snapshot with particles color coded according to their z-position. It is clear that the particles are ordered in lanes that alternate in height, and that these lanes slide past each other during the shear. To our knowledge, this phase has not been reported previously in the experimental literature. Although this phase melts back to a fluid phase in $\sim 3\ \tau_B$, it was experimentally possible to acquire 3D coordinates and a comparison of the calculated structure factor $S(\mathbf{q})$ at the equilibrium position of the oscillation cycle, as is shown in Fig. 9D and Fig. 9E. The corresponding real-space data are shown in Fig. 9F–I, where both crystal and fluid-like particles are reduced in diameter, except in the insets, which show the crystal-like particles at their original size. The ordering in the gradient–velocity plane (Fig. 9F–G) resembles the fcc(100) plane, with the

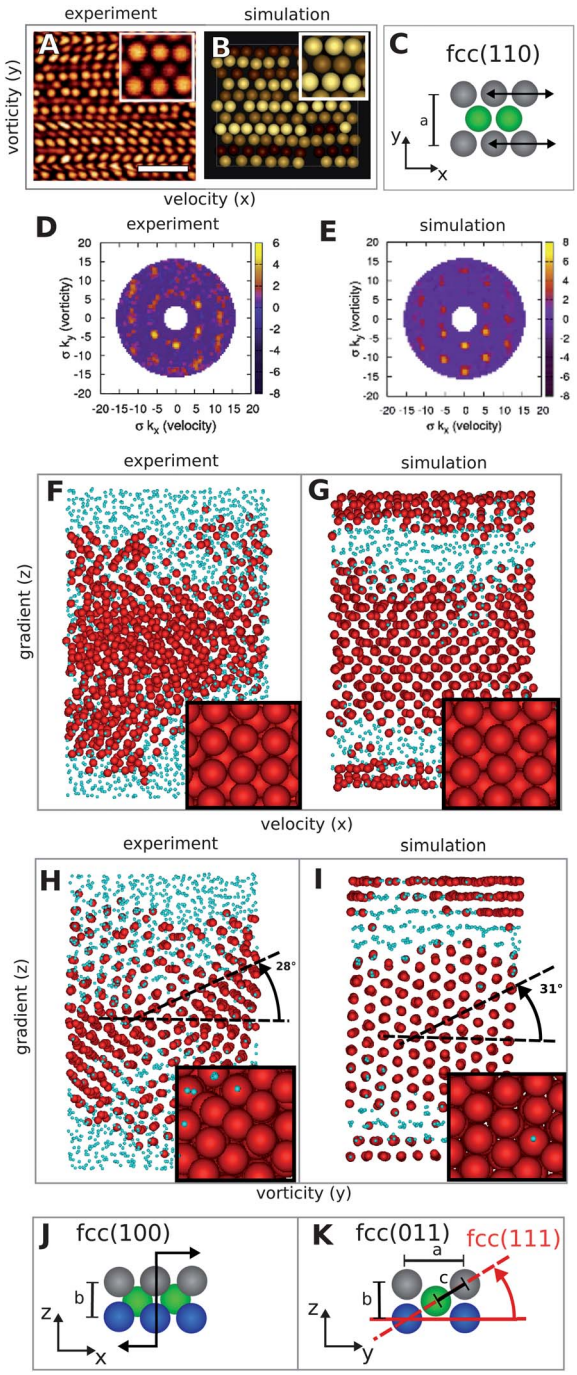

Fig. 9 The tilted layer phase. Experimental results for $\gamma_{max} = 0.65$, and $\phi = 0.50 \pm 0.01$, simulation for $\gamma_{max} = 0.9$ and $\phi = 0.48$. In both cases $Pe = 15$. (A) Confocal image during the shear with the inset showing the particles directly after cessation of the shear. The scale bar is 10 μm. (B) Simulation snapshot with particles color coded depending on their z-position. (C) Schematic model. Calculated 3D structure factors $S(\mathbf{q})$ for (D) experiment and (E) simulation. (F, G) Ordering in the gradient-velocity plane is similar to fcc(100). (H, I) The gradient-vorticity plane resembles an fcc(011) plane. (J, K) Schematic model of movement during the shear.

[011]-direction parallel to the velocity, as schematically depicted in Fig. 9J. The ordering in the gradient–vorticity plane (Fig. 9H–I) is similar to the fcc(011) plane, as depicted in Fig. 9K, which

leaves the velocity–vorticity plane with the same symmetry as the fcc(110) plane (Fig. 9A–B). In a perfect fcc(011) plane, the ratio of distances a and b in Fig. 9K is $a : b = \sqrt{2}$ and the red dotted line indicates the hexagonal fcc(111) plane that is perpendicular to the page and at an angle of 35° below the horizontal. As can be seen in Fig. 9H–I the angles of inclination are slightly lower than this value, close to 30°, which is the value for a perfect hexagonal ordering of the lanes. From these observations we conclude that the phase that is formed at the equilibrium position of the oscillation is a distorted fcc phase with its fcc(111) plane under an angle and therefore we refer to it as the 'tilted layer' phase. This phase was also observed when the plates were coated with polydisperse particles (polydispersity $\delta > 20\%$) so we do not think that the flatness of the plates is important. It is important to note that the value of the angle was not constant but depended on the number of oscillations, Peclet number and in the simulations also depended on the box size.

In Fig. 9 K, particles can freely slide until $c = b = \sigma$, corresponding to a volume fraction of $\phi = 0.605$. This implies that the tilted layer phase should also be observable in shear melted hard-sphere suspensions that are crystalline in equilibrium ($\phi > 0.54$). Based on the strong agreement in structure found in the experiments and simulations, we conclude that hydrodynamic interactions or non-linear flow profiles do not have a strong effect on the behavior of the particles because the simulation algorithm neglects hydrodynamics and imposes a linear velocity profile on the system.

Phase diagram

Multiple experiments and computer simulations were performed for varying strain amplitude and three fixed oscillation frequencies, resulting in the out-of-equilibrium phase diagrams in Fig. 10. The markers indicate the phases that were observed after a fixed number of 200 oscillations. After each experimental measurement, the sample was shear melted before the start of a new one by the application of a shear rate $\dot{\gamma}_{max} = 60\ s^{-1}$ and a strain amplitude $\gamma_{max} = 20$. To avoid shear history effects due to ordering at the walls, the glass slides were either coated with polydisperse particles or with two disordered layers of monodisperse particles. In the experiments (Fig. 10A), the crystal-like phases were always observed together with a fluid phase. For both the oscillating fcc and sliding layer phases, domains with deviating alignments were always present. The transitions between the crystal-like phases were not sharp and the markers indicate the predominant phase. The transition between the twinned fcc and sliding layered phases occurred at $\gamma_{max} \approx 0.5$, which is similar to the pioneering light scattering experiments by Ackerson *et al.*[3] and similar to the values found for suspensions that are crystalline in equilibrium.[10,14] The transition strain value was independent of the applied frequency range. The string phases were observed in samples with volume fractions $\phi = 0.47 \pm 0.01$ and $\phi = 0.46 \pm 0.01$, while all other observations are made at volume fractions of $\phi = 0.49 \pm 0.01$, where strings were not observed. The phase diagram determined from the simulations (Fig. 10B) is similar to the experimental phase diagram. The transition between the twinned fcc phase and the sliding layer phase occurred at the same strain amplitude ($\gamma_{max} \approx 0.5$), and was also independent of frequency. For $Pe > 5$ (upper right corner of the phase diagram) tilted layers were systematically observed in combination with sliding layers or string-like ordering. The ordering in the simulations did persist for larger strain amplitudes compared to the experiments. It is highly likely that the absence of hydrodynamic interactions in the simulations promotes the consistent layering of the sample even at strain amplitudes where in the experiments fluid order was found.

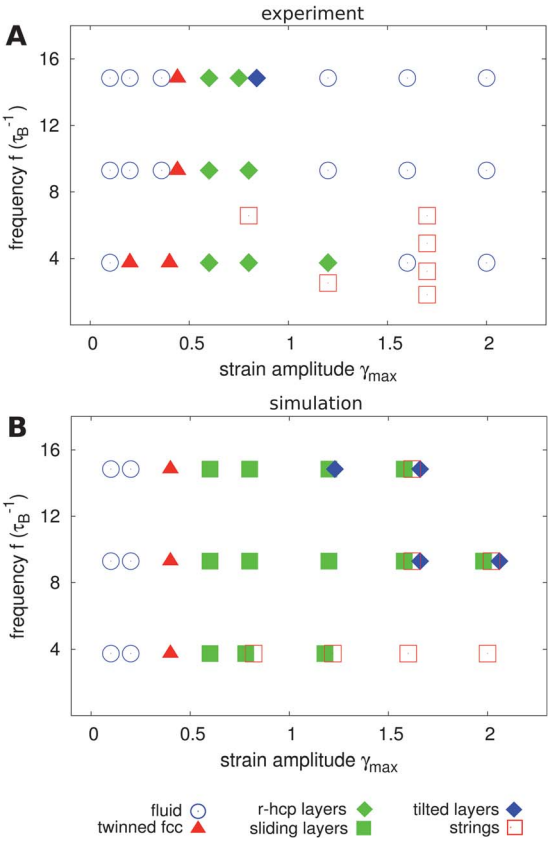

Fig. 10 The out-of-equilibrium phase diagrams showing the dominant structures induced after 200 oscillations. (A) Experimental results for samples with volume fraction $\phi = 0.49 \pm 0.01$. The string phases were observed in samples with volume fractions $\phi = 0.47 \pm 0.01$ and $\phi = 0.46 \pm 0.01$. (B) Simulation results for fixed volume fraction $\phi = 0.48$.

Conclusion

With both Brownian Dynamics simulations (without hydrodynamic interactions and an enforced linear shear profile) and experiments on PMMA colloids we have investigated and characterized the real-space structure of four oscillatory shear-induced phases in hard-sphere fluids. The experimentally observed ordering in the velocity–vorticity plane was in good agreement with the simulation results, but subtle differences were found in the three-dimensional order because the particles rearrange directly after cessation of the shear. Three phases correspond to existing light scattering experiments: an oscillating twinned fcc phase, a sliding layer phase and a string phase. The fourth shear-induced phase was not reported previously and because both experiments and simulations reveal a (distorted) fcc phase with hexagonal layers that are under an angle with the horizontal, we call it the tilted layer phase. Previous work by Wu

et al.[33] showed that the velocity profile of a partially crystallized (or sliding layer) suspension deviates from linearity, and that the local shear rate is approximately 1.5 times higher in the layered region than in the fluid phase. We expect similar effects in the current system because the crystal phases in this work were always observed together with a fluid phase. However, because the structures obtained from simulation (where a linear velocity profile was imposed on the system) are in strong agreement with the experiments, we conclude that deviations from a linear profile can be neglected in this work. Based on the same agreement, we also conclude that, except for large Peclet numbers, hydrodynamic interactions do not strongly affect the shear-induced structures.

Acknowledgements

We thank Johan Stiefelhagen for particle synthesis and Nick Koumakis for useful discussions. This research was carried out partially (THB) under project number M62.7.08SDMP25 in the framework of the Industrial Partnership Program on Size Dependent Material Properties of the Materials innovation institute (M2i) and the Foundation for Fundamental Research on Matter (FOM), which is part of the Netherlands Organization for Scientific Research. AF acknowledges the Deutsche Forschungsgemeinschaft (DFG) for financial support from SFB840/A3. MD acknowledges financial support from an NWO-VICI-grant and THB thanks the SFB-TR6 for a travel grant.

References

1 J. Vermant and M. J. Solomon, *J. Phys.: Condens. Matter*, 2005, **17**, R187.
2 B. J. Ackerson, *Phys. Rev. Lett.*, 1988, **61**, 1033.
3 B. J. Ackerson, *J. Rheol.*, 1990, **34**, 553.
4 N. Koumakis, A. B. Schofield and G. Petekidis, *Soft Matter*, 2008, **4**, 2008.
5 N. Duff and D. Lacks, *Phys. Rev. E: Stat., Nonlinear, Soft Matter Phys.*, 2007, **75**, 1.
6 X. Cheng, J. H. McCoy, J. N. Israelachvili and I. Cohen, *Science*, 2011, **333**, 1276.
7 X. Cheng, X. Xu, S. A. Rice, A. R. Dinner and I. Cohen, *Proc. Natl. Acad. Sci. U. S. A.*, 2011, **109**, 63.
8 Y. Yan, J. Dhont, C. Smits and H. Lekkerkerker, *Phys. A*, 1994, **202**, 68.
9 S. E. Paulin, B. J. Ackerson and M. S. Wolfe, *J. Colloid Interface Sci.*, 1996, **178**, 251.
10 M. D. Haw, W. C. K. Poon and P. N. Pusey, *Phys. Rev. E: Stat. Phys., Plasmas, Fluids, Relat. Interdiscip. Top.*, 1998, **57**, 6859.
11 I. Cohen, T. G. Mason and D. A. Weitz, *Phys. Rev. Lett.*, 2004, **93**.
12 T. Solomon and M. J. Solomon, *J. Chem. Phys.*, 2006, **124**, 134905.
13 I. Cohen, B. Davidovitch, A. B. Schofield, M. P. Brenner and D. A. Weitz, *Phys. Rev. Lett.*, 2006, **97**.
14 J. M. McMullan and N. J. Wagner, *J. Rheol.*, 2009, **53**, 575.
15 D. Derks, Y. L. Wu, A. van Blaaderen and A. Imhof, *Soft Matter*, 2009, **5**, 1060.
16 J. Delhommelle, J. Petravic and D. J. Evans, *J. Chem. Phys.*, 2004, **120**, 6117.
17 H. Komatsugawa and S. Nosé, *Phys. Rev. E: Stat. Phys., Plasmas, Fluids, Relat. Interdiscip. Top.*, 1995, **51**, 5944.
18 J. J. Erpenbeck, *Phys. Rev. Lett.*, 1984, **52**, 1333.
19 J. Delhommelle, J. Petravic and D. J. Evans, *Phys. Rev. E: Stat. Phys., Plasmas, Fluids, Relat. Interdiscip. Top.*, 2003, **68**, 031201.
20 J. Delhommelle, *Phys. Rev. E: Stat., Nonlinear, Soft Matter Phys.*, 2005, **71**, 016705.
21 P. D'Haene, J. Mewis and G. G. Fuller, *J. Colloid Interface Sci.*, 1993, **156**, 350.
22 W. Xue and G. S. Grest, *Phys. Rev. Lett.*, 1990, **64**, 419.
23 S. Butler and P. Harrowell, *J. Chem. Phys.*, 1996, **105**, 605.
24 G. Bosma, C. Pathmamanoharan, E. H. A. de Hoog, W. K. Kegel, A. van Blaaderen and H. N. W. Lekkerkerker, *J. Colloid Interface Sci.*, 2002, **245**, 292.
25 M. Leunissen, Ph.D. thesis, University Utrecht (2007).
26 A. Yethiraj and A. van Blaaderen, *Nature*, 2003, **421**, 513.
27 P. N. Pusey and W. van Megen, *Nature*, 1986, **320**, 340.
28 Y. L. Wu, J. H. J. Brand, J. L. A. van Gemert, J. Verkerk, H. Wisman, A. van Blaaderen and A. Imhof, *Rev. Sci. Instrum.*, 2007, **78**, 103902.
29 In the experimental literature on shear usually a 'peak to peak' distance for the strain amplitude in used, which is *twice* the value of the strain amplitude defined in rheology. In this work the latter definition is chosen.
30 J. C. Crocker and D. G. Grier, *J. Colloid Interface Sci.*, 1996, **179**, 298.
31 U. Dassanayake, S. Fraden and A. van Blaaderen, *J. Chem. Phys.*, 2000, **112**, 3851.
32 D. Ermak, *J. Chem. Phys.*, 1975, **62**.
33 Y. L. Wu, D. Derks, A. van Blaaderen and A. Imhof, *Proc. Natl. Acad. Sci. U. S. A.*, 2009, **106**, 10564.
34 J. F. Brady, *Chem. Eng. Sci.*, 2001, **56**, 2921.
35 P. Steinhardt, D. Nelson and M. Ronchetti, *Phys. Rev. B*, 1983, **28**, 784.
36 P. ten Wolde, M. J. Ruiz-Montero and D. Frenkel, *Phys. Rev. Lett.*, 1995, **75**, 2714.

Addition and correction

View Online

Note from RSC Publishing

This article was originally published with incorrect page numbers. This is the corrected, final version.

The Royal Society of Chemistry apologises for these errors and any consequent inconvenience to authors and readers.